Ultrafast, broadband, and configurable midinfrared all-optical switching in nonlinear graphene plasmonic waveguides

Ooi, Kelvin J.A.; Cheng, Jinluo; Sipe, J.e.; Ang, L.K.; Tan, Dawn T.H.

Published in:
APL Photonics

DOI:
10.1063/1.4948417

Publication date:
2016

Open . Published Online: June 2016Accepted: April 2016

Ultrafast, broadband, and configurable midinfrared all-optical switching in nonlinear graphene plasmonic waveguides

APL Photonics 1, 046101 (2016); https://doi.org/10.1063/1.4948417

Kelvin J. A. Ooi[1], J. L. Cheng[2], J. E. Sipe[3], L. K. Ang[1], *and* Dawn T. H. Tan[1, a)]

View Affiliations

Keywords
Keywords

- Plasmons
- Graphene
- Wave attenuation
- Nonlinear optical waveguides
- Optical pumping

ABSTRACT

Graphene plasmonics provides a unique and excellent platform for nonlinear all-optical switching, owing to its high nonlinear conductivity and tight optical confinement. In this paper, we show that impressive switching performance on graphene plasmonic waveguides could be obtained for both phase and extinction modulations at sub-MW/cm^2 optical pump intensities. Additionally, we find that the large surface-induced nonlinearity enhancement that comes from the tight confinement effect can potentially drive the propagating plasmon pump power down to the pW range. The graphene plasmonic waveguides have highly configurable Fermi-levels through electrostatic-gating, allowing for versatility in device design and a broadband optical response. The high capabilities of nonlinear graphene plasmonics would eventually pave the way for the adoption of the graphene plasmonics platform in future all-optical nanocircuitry.

Graphene is an atomically thin, honeycomb latticed material with a 2-dimensional band-structure. The rise of graphene since the 2000s has prompted widespread research in its various unique electronic and optical properties. In particular, there is growing interest in the field of graphene plasmonics due to its attractive tight optical confinement property, which allows extreme scaling of nanophotonic devices as well as increased light-matter interaction in the graphene medium.[1] In these recent few years, there were many theoretical and experimental demonstrations of graphene-based plasmonic photodetectors,[2–4] switches and modulators,[5–7]

logic gates,[8,9] light sources,[10–13] and polarizers and sensors.[14–17]

One of the major research areas in graphene is nonlinear photonics, which has seen applications in saturable absorbers,[18] nonlinear switching and solitons,[19–22] supercontinuum generation,[23] four-wave mixing,[24] and third-harmonic generation.[25] Measurements of graphene's Kerr nonlinearity have yielded very large values in several experiments.[24–27] However, in photonic-mode applications, the interaction of light with graphene is small due to weak confinement, thus the increase in nonlinearity is usually only by 1-order.[24] To achieve higher confinement factors, plasmonic-based optical structures could be deployed. Theoretically, it has been shown by Gorbach that the accessible nonlinearity by the plasmonic mode is easily 3 orders higher than that of the photonic mode.[22] In addition, due to surface-induced nonlinear enhancement, plasmonic pumps can further increase the nonlinearity by huge factors in orders of 10^{7}–10^{13}.[22]

There is also the concern of the graphene's material loss that scales with the confinement factor, which results in the degradation of nonlinear performance. In one paper,[28] it was pointed out that due to this trade-off, graphene's nonlinear performance is not superior to that of current existing nonlinear materials. However, we note that most of the present theoretical and experimental works paid more attention to the real part of the nonlinear refractive index.[24–32] Some of us have recently conducted an in-depth study of the nonlinearity of graphene by taking into

account the effects of finite temperature and phenomenological relaxation.[33] We found that the consideration of the imaginary part of the nonlinear index, i.e., the nonlinear absorption, would significantly change the evaluation of the nonlinear performance, which will be shown in detail in our analysis below.

There have been a number of recent studies[22,34–36] on surface-induced nonlinear enhancement effects on metal and graphene-based platforms. However, these studies only examine the effects of either the real or the imaginary part of the nonlinear of graphene separately. In this paper, we set out to assess the feasibility of nonlinear all-optical switching in graphene plasmonic waveguides through the consideration of both the real and imaginary parts of the nonlinear conductivity $\sigma^{(3)}$ and construct Figures-of-Merit (FoMs) for both phase-based and extinction-based optical switchings.

The biggest draw of nonlinear graphene plasmonics, apart from graphene's high $\sigma^{(3)}$, is the large optical confinement ability that enhances light-matter interaction in the graphene layer. On top of that, the optical confinement can be tailored for a large range of wavelengths through electrostatic tuning of the Fermi-level, something which is unseen of in metal-based plasmonics. This enables highly reconfigurable graphene plasmonic waveguides with respect to the operating wavelength λ_0.

A simple way to illustrate the optical confinement ability of surface plasmons is through the ratio of the transverse (E_T) and longitudinal (E_L) components of the electric-

field in the dielectric medium[37] – plasmons with a larger E_L component are better confined. The ratio for bulk metal plasmons is given by

$$\frac{E_T}{E_L} = i\frac{k_{sp}}{@k_{sp}^2 - I_d k_0^2} = i < \frac{a_P^2 - a^2}{I_d a^2}, \quad (1a)$$

where k_{sp} is the plasmon wave-vector, ε_d is the background medium permittivity, ω is the angular frequency, and ω_P is the plasma frequency of the metal. The transverse component is largely dominant due to the large ω_P of metal, with the exception when the operating frequency is near the surface plasmon resonance, i.e., at $\hat{a} = a_P/\sqrt{1 + I_d}$, which results in equal strength for both components.

Meanwhile, the ratio for graphene plasmons is written as

$$\frac{E_T}{E_L} = i\frac{k_{sp}}{@k_{sp}^2 - I_d k_0^2} = i < \sqrt{1 - \frac{1}{I_d}\left(\frac{U^{(1)}}{2I_0 c}\right)} \quad (1$$

whereby graphene's 2-dimensional optical conductivity is described by the Kubo formula[38]

$$U^{(1)} = \frac{ie^2 (2k_B T)}{\grave{U}\hbar^2 (\hat{a} + iU_1)} \{ \frac{E_F}{2k_B T} + \\ + \frac{ie^2}{4\hbar} \{ 0.5 + \tan^{-1} [\frac{\hbar (\hat{a} + iU_2) - 2|E_F|}{2k_B T}] -$$

where E_F is the Fermi-level of graphene at room temperature T = 300 K, $U_1 = ev_F^2/U_e E_F$ [39] and $v_2 \approx 0.8$ THz[18] are the relaxation frequencies for the intraband and interband

conductivities, respectively, $v_F = 10^6$ m/s is the Fermi velocity, and $\mu_e = 10^4$ cm^2/V s is the typical graphene's carrier mobility. Evaluating Eq. (2) will always yield $\sigma^{(1)} \ll \varepsilon_0 c$, even when E_F approaches 1.0 eV. Thus the ratio for graphene plasmons is unity in all cases, implying that the optical confinement for graphene plasmons is indeed very large.

We further verified the large optical confinement of graphene plasmons through COMSOL mode simulations. In Figure 1 we show the simulated optical mode profile for both gold and graphene. To simplify our studies, we do not consider phonon couplings which might be present in some substrates. Henceforth we use a background material of air, $\varepsilon_d = 1$, in our calculations. To facilitate a fair comparison, we fixed the waveguide dimensions to 0.5 μm × 3 Å and set λ_0 to 1.55 μm and graphene $E_F = 0.7$ eV, after considering the fact that gold does not display good plasmonic property in the midinfrared wavelength while graphene only exhibits plasmonic property at 1.55 μm when doped to >0.5 eV. The effective mode area, A_{eff}, is calculated for both cases. At the high confinement limit, where $E_T \approx iE_L$, A_{eff} for surface plasmons is written as[22]

$$A_{eff} = \frac{\left(\iint |E|^2 dxdy\right)^2}{\iint_{slab} \frac{1}{2}|E_L|^4 dxdy}, \tag{3}$$

where the electric-field in the numerator is evaluated over the whole waveguide and background, while in the denominator, it is evaluated only within the waveguide slab. We obtained A_{eff} in the order of 1 μm^2 for gold and 0.01 μm^2 for graphene, which confirmed the

validity of the simple assessment using Eqs. (1a) and (1b). It should be noted that the A_{eff} value of graphene at this wavelength and doping can also be easily obtained in the midinfrared when the E_F is adjusted accordingly.

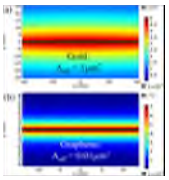

FIG. 1.

Electric-field distribution of a 0.5 μm × 3 Å waveguide for (a) gold and (b) graphene (E_F = 0.7 eV) for λ_0 = 1.55 μm. The background material is air, ε_d = 1.

PPT | High-resolution

In this paper, we only consider the Kerr effect of graphene, which is thought to be instantaneous. In our interested frequency range, the graphene electronic structure can be well approximated by a two-band tight binding model utilizing only the carbon $2p_z$ orbital, and then $\sigma^{(3)}$ (Kerr coefficients) are calculated employing a semiconductor Bloch equation approach,[32,33] taking into account phenomenological relaxation parameters for both the intraband and the interband transitions. At zero temperature and further taking the linear dispersion approximation around the Dirac points, we first extracted an analytic expression for $\sigma^{(3)}$ in the perturbation regime. The conductivities at room temperature are then obtained by an appropriate integration over the zero temperature results,[33] taking the intraband and

interband relaxation frequency values from Eq. (2).

The computed nonlinear conductivities for both real and imaginary parts in the midinfrared spectrum are shown in Figure 2. Across wavelengths, the variation of the nonlinearity is fairly constant within an order of magnitude. Across Fermi-levels, however, as the high Kerr nonlinearity of graphene originates from the electrons located at the Dirac point, the nonlinearity weakens when graphene is doped to a higher E_F. Variation of the nonlinear conductivity across E_F is large for the real part and small for the imaginary part; at low E_F, the real $\sigma^{(3)}$ dominates, and vice versa for the imaginary $\sigma^{(3)}$.

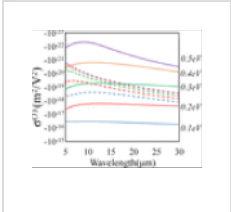

FIG. 2.

Real (solid lines) and imaginary (dashed lines) $\sigma^{(3)}$ of graphene with different E_F in the midinfrared.

PPT | High-resolution

Here we shall attempt to quantify the performance of graphene plasmonic nonlinear switching in the midinfrared regime. The usual way to characterize nonlinearity is through the third-order Kerr nonlinear susceptibility, $\chi^{(3)}$, which would then be formulated into the material nonlinear refractive index, n_2. The Kerr susceptibility can be obtained from the $\sigma^{(3)}$ through a simple expression $\chi^{(3)} = i\sigma^{(3)}/\varepsilon_0\omega\Delta$. Meanwhile, the complex refractive index is expressed as $n + ik = \sqrt{1 + iU^{(1)}/I_0\hat{a}\Delta}$,

where $\Delta = 3$ Å is the atomic thickness of graphene. Since graphene has a substantial linear absorption coefficient, we use the general formulation of the complex $n_2 + ik_2$,[40]

$$n_2 = \frac{3}{4I_0c\,(n^2+k^2)}\left[a_R^{(3)} + \frac{k}{n}a_I^{(3)}\right], \quad (4a)$$

$$k_2 = \frac{3}{4I_0c\,(n^2+k^2)}\left[a_I^{(3)} - \frac{k}{n}a_R^{(3)}\right]. \quad (4b)$$

The calculated n_2 and k_2 are plotted in Figures 3(a) and 3(b). n_2 is always negative due to $\chi_R^{(3)}$ and $\chi_I^{(3)}$ being negative, while k_2 is negative at low E_F, but crosses into the positive regime when $\chi_R^{(3)} \gg \chi_I^{(3)}$ at higher E_F.

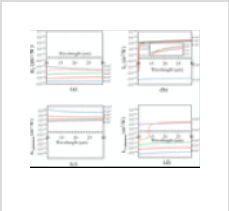

FIG. 3.

Nonlinear refractive indices (a) and (b), and nonlinear plasmon indices (c) and (d) for graphene with different E_F in the midinfrared.

PPT | High-resolution

The n_2 analysis above is, however, only useful when one considers the light energy impinging on the graphene surface. If light is coupled evanescently to the plasmonic modes which have parallel wave-vectors to the graphene surface, then the plasmonic waveguide index, $n_{plasmon}$, and its corresponding $n_{2\text{-plasmon}}$ have to be defined. In this case, we first consider the $n_{plasmon}$ of a graphene plasmonic waveguide

$$n_{plasmon} = \sqrt{I_d - \left(\frac{2I_dI_0c}{U^{(1)}}\right)^2}. \quad (5a)$$

Then, we define the $n_{plasmon}$ modulated by light with index-normalized, local intensity $I = cI_0|E|^2/2$,

$$n^{\$}_{plasmon} = \sqrt{I_d - \left(\frac{2I_d I_0 c}{U^{(1)} + \Delta\ddot{U}}\right)^2}, \qquad (5b)$$

where $\Delta\ddot{U} = 3U^{(3)}|E|^2/4 = 3U^{(3)}I/2cI_0$. After that, $n_{2\text{-}plasmon}$ could be easily defined through

$$n_{2\text{-}plasmon} = n_{plasmon}/I, \qquad (6a)$$

$$k_{2\text{-}plasmon} = k_{plasmon}/I, \qquad (6b)$$

where $n_{plasmon}$ and $k_{plasmon}$ represent the difference between the two plasmon indices in Eqs. (5a) and (5b), real and imaginary components, respectively. The calculated $n_{2\text{-}plasmon}$ and $k_{2\text{-}plasmon}$ are plotted in Figures 3(c) and 3(d). It is seen that their trends are markedly different from the material n_2 and k_2. $n_{2\text{-}plasmon}$ is always positive, indicating that optical confinement will always be increased upon modulation. Meanwhile, $k_{2\text{-}plasmon}$ is largely negative at lower E_F, which suggests that the graphene plasmonic waveguide has potential saturable absorption property.

The above analysis is valid for light intensities far below the threshold saturation intensity, $I \ll I_{th}$. For the full picture, it is necessary to define the optical conductivity modulation such that

$$\Delta\ddot{U} = \frac{3U^{(3)}}{2I_0 c} \cdot \frac{I}{1 + I/I_{th}}. \qquad (7a)$$

We adopt the definition of I_{th} as the optical intensity required to reduce the conductivity by half, i.e.,

(7b)

Hence, $$U^{(1)} + \frac{3U^{(3)} I_{th}}{4 I_0 c} = \frac{U^{(1)}}{2}.$$

$$I_{th,\mathrm{Re(Im)}} = -2 I_0 c \frac{U^{(1)}_{\mathrm{Re(Im)}}}{3U^{(3)}_{\mathrm{Re(Im)}}}. \quad (7c)$$

Figure 4 illustrates how (a) $n_{plasmon}$ and (b) $k_{plasmon}$ vary with the optical pump intensity for graphene with a few different Fermi-levels and at the wavelength of 20 μm. We see that the drop in $k_{plasmon}$ is steep even for intensities at the sub-MW/cm^2 level and then quickly saturates when the intensity approaches 1 MW/cm^2. In contrast, $n_{plasmon}$ displays only a slight linear increase in magnitude over this range. However, this does not mean that the phase-modulation performance is poor; any reasonable assessment should also take into account the large accompanying extension of the effective waveguide length, which will be discussed in more detail in the next paragraph.

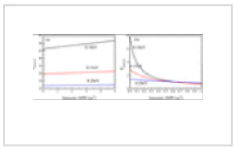

FIG. 4.

Variation of (a) $n_{plasmon}$ and (b) $k_{plasmon}$ with optical pump intensity at λ_0 = 20 μm.

The two possible modulation schemes for graphene plasmonic waveguides are through the phase and extinction changes. Here we consider a top-down illumination of the optical pump that modulates a propagating graphene plasmon signal. The FoM for the phase modulation is defined as

(8a)

where $L^{\$}_{plasmon} = \frac{a}{c} = \alpha/2\hat{a}\,\mathrm{Im}\,(n^{\$}_{plasmon})$, is the effective waveguide length after modulation. Meanwhile, the FoM for the extinction modulation is defined as

$$\frac{\Delta E}{E} = \frac{\mathrm{Im}\,(n^{\$}_{plasmon}) - \mathrm{Im}\,(n_{plasmon})}{\mathrm{Im}\,(n_{plasmon})}. \quad (8b)$$

Figure 5 shows the FoMs for the nonlinear phase and extinction modulation for graphene with respect to E_F, λ_0, and the optical pump intensity. For the nonlinear phase modulation at E_F = 0.1 eV depicted in Figure 5(a), an optical pump intensity of 1.5 MW/cm^2 is needed to induce a π phase-shift for a broad range of wavelengths. A 2.5-fold increase of optical pump intensity to 3.75 MW/cm^2 is required to induce the π phase-shift if E_F is raised to 0.15 eV, as shown in Figure 5(b).

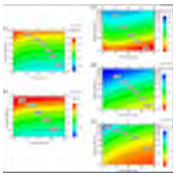

FIG. 5.

Nonlinear phase-change for E_F of (a) 0.1 eV, and (b) 0.15 eV; and nonlinear extinction-change for E_F of (c) 0.1 eV, (d) 0.15 eV, (e) 0.2 eV modulated by various levels of optical pump intensity in the midinfrared.

PPT | High-resolution

Meanwhile, for nonlinear extinction modulation shown in Figures 5(c)–5(e), 80% loss modulation is achievable for an optical pump intensity as low as 0.4 MW/cm^2 at E_F = 0.1 eV. The nature of the loss modulation is the

reduction in propagation losses due to saturable absorption. The performance deteriorates to ~30% when the E_F is doubled to 0.2 eV. The FoM of the extinction modulation would impact the switching characteristics in terms of insertion loss (IL), extinction loss (EL), and extinction ratio (ER). For example, if one were to design an extinction modulator with an ER of 3 dB, then an FoM of −80% would translate to a 0.75 dB IL and 3.75 dB EL.

For a propagating optical pump (e.g., in self-phase modulation or cross-phase modulation), as the pump itself is a graphene plasmon, we can further analyse the effect of the optical mode on the optical switching performance. The relation of the optical power and the optical intensity is given by

$$P_0 = I_0 \times A_{eff} = \frac{1}{g} \cdot \frac{I \times A_{eff}}{n_{plasmon}}, \qquad (9)$$

where I_0 is the free-space optical intensity, related to the local intensity by $I = I_0 \times n_{plasmon}$. A_{eff} is calculated based on the 0.5 μm × 3 Å waveguide dimension. There is a large variation in the $A_{eff}/n_{plasmon}$ factor, by up to 6-orders, as shown in Figures 6(a) and 6(b). Confinement of the graphene plasmon modes is tight at the low E_F and short λ_0 regime, and vice versa. Furthermore, there is a surface-induced nonlinear enhancement factor that scales in the order of $g \approx 4n_{plasmon}^4$,[22] which drastically reduces the required pump power if $n_{plasmon}$ is very large. If we assume that the optical pump is coupled from free-space optics through phase-matching techniques (e.g., dielectric gratings[41]), and the coupling efficiency is naively assumed to be 1%, then

the optical pump power could be simply estimated by multiplying the pump intensity with the $A_{eff}/n_{plasmon}/g$ scaling factor. As an illustration, in Figures 6(c) and 6(d), we show the optical pump power required for phase and extinction modulations respectively, for graphene with a Fermi-level E_F = 0.1 eV. Clearly, performance is better at the shorter wavelengths for both types of modulation, due to the larger confinement that reduces A_{eff} and increases $n_{plasmon}$ and g, thereby greatly reducing the scaling factor. From calculations, for a λ_0 = 10 μm signal at E_F = 0.1 eV ($n_{plasmon}$ = 68), 13 pW is required for a π phase-shift, while only 4.8 pW is required for a −80% extinction modulation.

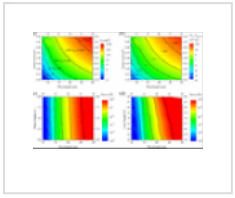

FIG. 6.

(a) Effective Mode Area, A_{eff}, and (b) normalized A_{eff} by $n_{plasmon}$ of graphene with respect to various E_F in the midinfrared. (c) and (d) Optical pump power required for phase and extinction modulation respectively, for graphene E_F = 0.1 eV.

PPT | High-resolution

As an overall assessment of the phase and extinction modulation efficiency, the performance is generally better for short λ_0 and low E_F, a conclusion which is similarly reached in our previous studies on its electro-optic modulation counterpart.[7,8] Compared to metal-based plasmonics and dielectrics,[42–44] the performance of graphene is vastly superior,

while closely rivalling that of Epsilon-Near-Zero-based materials like AZO.[45] While there are efforts to increase the modulation strength in all-optical metal-based plasmonics through employment of resonant structures,[43,44] the bandwidth is ultimately sacrificed, in contrast to graphene where the operating wavelength can be highly broadband from $\lambda_0 = 10–30\ \mu$m. For example, the switching powers in the long-range metal plasmonic waveguides studied by Baron *et al.*[42] are on the order of kW/mm, due to the very low optical confinement. And a nonlinear switch based on a silicon plasmonic ring resonator, studied by Sederberg *et al.*,[43] requires operating powers as high as 290 mW, and the device has a free-spectral range of only about 0.2 μm.

On the other hand, utilizing the plasmonic platform also greatly increases the nonlinearity of graphene through the surface-induced nonlinear enhancement effects. One example is in non-plasmonic graphene saturable absorbers, where saturable absorption occurs at peak-powers as high as 1 W.[46] In comparison, we have shown that graphene plasmonic waveguides can achieve saturable absorption for pump powers in the pW range.

Graphene plasmonics is an attractive nonlinear platform not only due to its high $\sigma^{(3)}$, but also its tight optical confinement ability which enhances light-matter interaction. In this paper, we studied the performance of nonlinear all-optical switching for graphene plasmons. Analysis reveals that top-down illuminating optical pump intensities of 0.4–1.5 MW/cm^2 are enough to induce a π phase-shift

and 80% modulation for phase and extinction switchings, respectively. On the other hand, due to the surface-enhanced nonlinear effect, propagating plasmon pumps require very low powers to perform optical switching in the order of pW. Furthermore, the device response is fully broadband from 10 to 30 μm. Last but not least, the fully electrostatic configurability of graphene's E_F allows the device to be tailored to any wavelength response and benchmark performance as one desires.

The exciting performance figures of nonlinear graphene plasmonics give an optimistic outlook on the design of power-efficient and broadband all-optical graphene plasmonic devices. The huge performance merits coupled with design versatility and advantageous size-integration factor will eventually herald the adoption of the graphene plasmonics in future all-optical nanocircuit platforms.

This work was supported by the MOE ACRF Tier 2 grant, SUTD–MIT International Design Center, and SUTD–ZJU collaborative research grant. J.L.C. acknowledges the support from EU-FET Grant GRAPHENICS (No. 618086), the ERC-FP7/2007-2013 Grant No. 336940, and the FWO-Vlaanderen Project No. G.A002.13N.

REFERENCES

1.
A. N. Grigorenko, M. Polini, and K. Novoselov, "Graphene plasmonics," Nat. Photonics **6**, 749–758 (2012).
https://doi.org/10.1038/nphoton.2012.262,
Google Scholar, Crossref, CAS

2.
F. Xia, T. Mueller, Y. M. Lin, A. Valdes-Garcia, and P. Avouris, "Ultrafast graphene photodetector," Nat. Nanotechnol. **4**, 839–843 (2009).
https://doi.org/10.1038/nnano.2009.292,
Google Scholar, Crossref, CAS

3.
J. T. Kim, Y.-J. Yu, H. Choi, and C.-G. Choi, "Graphene-based plasmonic photodetector for photonic integrated circuits," Opt. Express **22**, 803–808 (2014).
https://doi.org/10.1364/OE.22.000803,
Google Scholar, Crossref

4.
F. H. L. Koppens, T. Mueller, P. Avouris, A. C. Ferrari, M. S. Vitiello, and M. Polini, "Photodetectors based on graphene other two-dimensional materials and hybrid systems," Nat. Nanotechnol. **9**, 780–793 (2014).
https://doi.org/10.1038/nnano.2014.215,
Google Scholar, Crossref, CAS

5.
D. R. Andersen, "Graphene-based long-wave infrared TM surface plasmon modulator," J. Opt. Soc. Am. B **27**, 818–823 (2010).
https://doi.org/10.1364/JOSAB.27.000818,
Google Scholar, Crossref, CAS

6.

J. Gosciniak and D. T. H. Tan, "Graphene-based waveguide integrated dielectric-loaded plasmonic electro-absorption modulators," Nanotechnology **24**, 185202 (2013). https://doi.org/10.1088/0957-4484/24/18/185202
, Google Scholar, Crossref

7.
K. J. A. Ooi, H. S. Chu, L. K. Ang, and P. Bai, "Mid-infrared active graphene nanoribbon plasmonic waveguide devices," J. Opt. Soc. Am. B **30**, 3111–3116 (2013). https://doi.org/10.1364/JOSAB.30.003111, Google Scholar, Crossref, CAS

8.
K. J. A. Ooi, H. S. Chu, P. Bai, and L. K. Ang, "Electro-optical graphene plasmonic logic gates," Opt. Lett. **39**, 1629–1632 (2014). https://doi.org/10.1364/OL.39.001629, Google Scholar, Crossref, CAS

9.
B. Zhu, G. Ren, Y. Gao, B. Wu, C. Wan, and S. Jian, "Magnetically-controlled logic gates of graphene plasmons based on non-reciprocal coupling," IEEE J. Sel. Top. Quantum Electron. **22**, 1–7 (2016). https://doi.org/10.1109/JSTQE.2016.2537209, Google Scholar, Crossref, CAS

10.

S. Liu, C. Zhang, M. Hu, X. Chen, P. Zhang, S. Gong, T. Zhao, and R. Zhong, "Coherent and tunable terahertz radiation from graphene surface plasmon polaritons excited by an electron beam," Appl. Phys. Lett. **104**, 201104 (2014). https://doi.org/10.1063/1.4879017, Google Scholar, Scitation

11.
R. Beams, P. Bharadwaj, and L. Novotny, "Electroluminescence from graphene excited by electron tunnelling," Nanotechnology **25**, 055206 (2014). https://doi.org/10.1088/0957-4484/25/5/055206
, Google Scholar, Crossref

12.
K. J. A. Ooi, W. S. Koh, H. S. Chu, D. T. H. Tan, and L. K. Ang, "Efficiencies of aloof-scattered electron beam excitation of metal and graphene plasmons," IEEE Trans. Plasma Sci. **43**, 951–956 (2015). https://doi.org/10.1109/TPS.2014.2379259, Google Scholar, Crossref, CAS

13.
K. J. A. Ooi, H. S. Chu, C. Y. Hsieh, D. T. H. Tan, and L. K. Ang, "Highly efficient midinfrared on-chip electrical generation of graphene plasmons by inelastic electron tunnelling excitation," Phys. Rev. Appl. **3**, 054001 (2015). https://doi.org/10.1103/PhysRevApplied.3.054001
, Google Scholar, Crossref

14.

Q. Bao, H. Zhang, B. Wang, Z. Ni, C. H. Y. X. Lim, Y. Wang, D. Y. Tang, and K. P. Loh, "Broadband graphene polarizer," Nat. Photonics **5**, 411–415 (2011). https://doi.org/10.1038/nphoton.2011.102, Google Scholar, Crossref, CAS

15.
J. T. Kim and C.-G. Choi, "Graphene-based polymer waveguide polarizer," Opt. Express **20**, 3556–3562 (2012). https://doi.org/10.1364/OE.20.003556, Google Scholar, Crossref, CAS

16.
L. Wu, H. S. Chu, W. S. Koh, and E. P. Li, "Highly sensitive graphene biosensors based on surface plasmon resonance," Opt. Express **18**, 14395–14400 (2010). https://doi.org/10.1364/OE.18.014395, Google Scholar, Crossref, CAS

17.
D. Rodrigo, O. Limaj, D. Janner, D. Etezadi, F. J. García de Abajo, V. Pruneri, and H. Altug, "Mid-infrared plasmonic biosensing with graphene," Science **349**, 165–168 (2015). https://doi.org/10.1126/science.aab2051, Google Scholar, Crossref, CAS

18.

Q. Bao, H. Zhang, Y. Wang, Z. Ni, Y. Yan, Z. X. Shen, K. P. Loh, and D. Y. Tang, "Atomic-layer graphene as a saturable absorber for ultrafast pulsed lasers," Adv. Funct. Mater. **19**, 3077–3083 (2009). https://doi.org/10.1002/adfm.200901007, Google Scholar, Crossref, CAS

19.
M. L. Nesterov, J. Bravo-Abad, A. Yu. Nikitin, F. J. García-Vidal, and L. Martin-Moreno, "Graphene supports the propagation of subwavelength optical solitons," Laser Photonics Rev. **7**, L7–L11 (2013). https://doi.org/10.1002/lpor.201200079, Google Scholar, Crossref, CAS

20.
K. J. A. Ooi, L. K. Ang, and D. T. H. Tan, "Waveguide engineering of graphene's nonlinearity," Appl. Phys. Lett. **105**, 111110 (2014). https://doi.org/10.1063/1.4895934, Google Scholar, Scitation

21.
D. Chatzidimitriou, A. Pitilakis, and E. E. Kriezis, "Rigorous calculation of nonlinear parameters in graphene-comprising waveguides," J. Appl. Phys. **118**, 023105 (2015). https://doi.org/10.1063/1.4926501, Google Scholar, Scitation

22.

A. V. Gorbach, "Nonlinear graphene plasmonics: Amplitude equation for surface plasmons," Phys. Rev. A **87**, 013830 (2013). https://doi.org/10.1103/PhysRevA.87.013830, Google Scholar, Crossref

23.
A. V. Gorbach, "Graphene plasmonic waveguides for mid-infrared supercontinuum generation on a chip," Photonics **2**, 825–837 (2015). https://doi.org/10.3390/photonics2030825, Google Scholar, Crossref, CAS

24.
T. Gu, N. Petrone, J. F. McMillan, A. van der Zande, M. Yu, G. Q. Lo, D. L. Kwong, J. Hone, and C. W. Wong, "Regenerative oscillation and four-wave mixing in graphene optoelectronics," Nat. Photonics **6**, 554–559 (2012). https://doi.org/10.1038/nphoton.2012.147, Google Scholar, Crossref, CAS

25.
S.-Y. Hong, J. I. Dadap, N. Petrone, P.-C. Yeh, J. Hone, and R. M. Osgood, Jr., "Optical third-harmonic generation in graphene," Phys. Rev. X **3**, 021014 (2013). https://doi.org/10.1103/physrevx.3.021014, Google Scholar, Crossref

26.

E. Hendry, P. J. Hale, J. Moger, A. K. Savchenko, and S. A. Mikhailov, "Coherent nonlinear optical response of graphene," Phys. Rev. Lett. **105**, 097401 (2010). https://doi.org/10.1103/PhysRevLett.105.097401
, Google Scholar, Crossref, CAS

27.
H. Zhang, S. Virally, Q. Bao, K. P. Loh, S. Massar, N. Godbout, and P. Kockaert, "Z-scan measurement of the nonlinear refractive index of graphene," Opt. Lett. **37**, 1856–1858 (2012). https://doi.org/10.1364/OL.37.001856,
Google Scholar, Crossref, CAS

28.
J. B. Khurgin, "Graphene—A rather ordinary nonlinear optical material," Appl. Phys. Lett. **104**, 161116 (2014). https://doi.org/10.1063/1.4873704,
Google Scholar, Scitation

29.
A. R. Wright, X. G. Xu, J. C. Cao, and C. Zhang, "Strong nonlinear optical response in graphene in terahertz regime," Appl. Phys. Lett. **95**, 072101 (2009). https://doi.org/10.1063/1.3205115,
Google Scholar, Scitation

30.
Y. S. Ang, S. Sultan, and C. Zhang, "Nonlinear optical spectrum of bilayer graphene in the terahertz regime," Appl. Phys. Lett. **97**, 243110 (2010). https://doi.org/10.1063/1.3527934,
Google Scholar, Scitation

31.
S. Sultan, Y. S. Ang, and C. Zhang, "Room temperature strong terahertz photon mixing in graphene," J. Opt. Soc. Am. B **29**, 274 (2012). https://doi.org/10.1364/josab.29.000274, Google Scholar, Crossref

32.
J. L. Cheng, N. Vermeulen, and J. E. Sipe, "Third order optical nonlinearity of graphene," New J. Phys. **16**, 053014 (2014). https://doi.org/10.1088/1367-2630/16/5/053014
, Google Scholar, Crossref

33.
J. L. Cheng, N. Vermeulen, and J. E. Sipe, "Third-order nonlinearity of graphene: Effects of phenomenological relaxation and finite temperature," Phys. Rev. B **91**, 235320 (2015). https://doi.org/10.1103/PhysRevB.91.235320, Google Scholar, Crossref

34.
B. Simkhovich and G. Bartal, "Plasmon-enhanced four-wave mixing for superresolution applications," Phys. Rev. Lett. **112**, 056802 (2014). https://doi.org/10.1103/PhysRevLett.112.056802
, Google Scholar, Crossref

35.

X. Yao, M. Tokman, and A. Belyanin, "Efficient nonlinear generation of THz plasmons in graphene and topological insulators," Phys. Rev. Lett. **112**, 055501 (2014). https://doi.org/10.1103/PhysRevLett.112.055501
, Google Scholar, Crossref

36.
S. Thongrattanasiri, F. H. L. Koppens, and F. J. García de Abajo, "Complete optical absorption in periodically patterned graphene," Phys. Rev. Lett. **108**, 047401 (2012). https://doi.org/10.1103/PhysRevLett.108.047401
, Google Scholar, Crossref

37.
A. V. Zayats, I. I. Smolyaninov, and A. A. Maradudin, "Nano-optics of surface plasmon polaritons," Phys. Rep. **408**, 131–314 (2005). https://doi.org/10.1016/j.physrep.2004.11.001
, Google Scholar, Crossref, CAS

38.
L. A. Falkovsky, "Optical properties of graphene," J. Phys.: Conf. Ser. **129**, 012004 (2008). https://doi.org/10.1088/1742-6596/129/1/012004
, Google Scholar, Crossref

39.

M. Jablan, H. Buljan, and M. Soljačić, "Plasmonics in graphene at infrared frequencies," Phys. Rev. B **80**, 245435 (2009). https://doi.org/10.1103/PhysRevB.80.245435, Google Scholar, Crossref

40.
R. del Coso and J. Solis, "Relation between nonlinear refractive index and third-order susceptibility in absorbing media," J. Opt. Soc. Am. B **21**, 640–644 (2004). https://doi.org/10.1364/JOSAB.21.000640, Google Scholar, Crossref, CAS

41.
W. Gao, J. Shu, C. Qiu, and Q. Xu, "Excitation of plasmonic waves in graphene by guided-mode resonances," ACS Nano **6**, 7806–7813 (2012). https://doi.org/10.1021/nn301888e, Google Scholar, Crossref, CAS

42.
A. Baron, S. Larouche, D. J. Gauthier, and D. R. Smith, "Scaling of the nonlinear response of the surface plasmon polariton at a metal/dielectric interface," J. Opt. Soc. Am. B **32**, 9–14 (2015). https://doi.org/10.1364/JOSAB.32.000009, Google Scholar, Crossref, CAS

43.
S. Sederberg, D. Driedger, M. Nielsen, and A. Y. Elezzabi, "Ultrafast all-optical switching in a silicon-based plasmonic nanoring resonator," Opt. Express **23**, 23494–23503 (2011). https://doi.org/10.1364/OE.19.023494, Google Scholar, Crossref

44.
Y. Xu, X. Wang, H. Deng, and K. Guo, "Tunable all-optical plasmonic rectifier in nanoscale metal–insulator–metal waveguides," Opt. Lett. **39**, 5846–5849 (2014).
https://doi.org/10.1364/OL.39.005846,
Google Scholar, Crossref, CAS

45.
N. Kinsey, C. DeVault, J. Kim, M. Ferrera, V. M. Shalaev, and A. Boltasseva, "Epsilon-near-zero Al-doped ZnO for ultrafast switching at telecom wavelengths," Optica **2**, 616–622 (2015).
https://doi.org/10.1364/OPTICA.2.000616,
Google Scholar, Crossref, CAS

46.
C. Meng, S. L. Yu, H. Q. Wang, Y. Cao, L. M. Tong, W. T. Liu, and Y. R. Shen, "Graphene-doped polymer nanofibers for low-threshold nonlinear optical waveguiding," Light Sci. Appl. **4**, e348 (2015).
https://doi.org/10.1038/lsa.2015.121,
Google Scholar, Crossref, CAS